JCI insight

RESEARCH ARTICLE

Increased FGF23 protects against detrimental cardio-renal consequences during elevated blood phosphate in CKD

Erica L. Clinkenbeard,[1] Megan L. Noonan,[1] Joseph C. Thomas,[1] Pu Ni,[1] Julia M. Hum,[1] Mohammad Aref,[2] Elizabeth A. Swallow,[2] Sharon M. Moe,[3] Matthew R. Allen,[2] and Kenneth E. White[1,2]

[1]Department of Medical and Molecular Genetics, [2]Department of Anatomy and Cell Biology, and [3]Division of Nephrology, Department of Medicine, Indiana University School of Medicine, Indianapolis, Indiana, USA.

The phosphaturic hormone FGF23 is elevated in chronic kidney disease (CKD). The risk of premature death is substantially higher in the CKD patient population, with cardiovascular disease (CVD) as the leading mortality cause at all stages of CKD. Elevated FGF23 in CKD has been associated with increased odds for all-cause mortality; however, whether FGF23 is associated with positive adaptation in CKD is unknown. To test the role of FGF23 in CKD phenotypes, a late osteoblast/osteocyte conditional flox-*Fgf23* mouse (*Fgf23*$^{fl/fl}$/*Dmp1*-Cre$^{+/-}$) was placed on an adenine-containing diet to induce CKD. Serum analysis showed casein-fed Cre^{+} mice had significantly higher serum phosphate and blood urea nitrogen (BUN) versus casein diet and Cre^{-} genotype controls. Adenine significantly induced serum intact FGF23 in the Cre^{-} mice over casein-fed mice, whereas Cre^{+} mice on adenine had 90% reduction in serum intact FGF23 and C-terminal FGF23 as well as bone *Fgf23* mRNA. Parathyroid hormone was significantly elevated in mice fed adenine diet regardless of genotype, which significantly enhanced midshaft cortical porosity. Echocardiographs of the adenine-fed Cre^{+} hearts revealed profound aortic calcification and cardiac hypertrophy versus diet and genotype controls. Thus, these studies demonstrate that increased bone FGF23, although associated with poor outcomes in CKD, is necessary to protect against the cardio-renal consequences of elevated tissue phosphate.

Introduction

Maintaining serum phosphate within a fairly narrow physiological range is critical for proper energy metabolism and prevents mineralization of soft tissues. Control of phosphate handling occurs through dietary absorption in the intestine, through renal reabsorption, and via long-term storage in the skeleton (1). Fibroblast growth factor-23 (FGF23) is a bone-produced hormone involved in maintaining phosphate balance through control of renal phosphate reabsorption and 1,25$(OH)_2$ vitamin D (1,25D) synthesis (2). After its release from osteoblasts/osteocytes in humans and rodent models of situations of hyperphosphatemia (3–5) or increased 1,25D (6), FGF23 binds to its coreceptor α-Klotho and an FGF receptor (FGFR) in the kidney (7, 8). FGF23 signaling reduces expression of the renal proximal tubule sodium-phosphate cotransporters NPT2a and NPT2c, increasing phosphate excretion (9, 10). To control 1,25D, the actions of FGF23 downregulation of renal vitamin D 1α-hydroxylase (*CYP27b1*), and increased expression of vitamin D 24-hydroxylase (*CYP24a1*), lead to a decrease in circulating 1,25D (9). Parathyroid hormone (PTH) has the same effect as FGF23 on tubular phosphate reabsorption, but converse effects on 1,25D production (11). Bone FGF23 mRNA expression and circulating concentrations are influenced by multiple factors including systemic changes in phosphate (5), 1,25D (6, 12), PTH (13), iron handling (14), inflammation (15, 16), as well as local factors including FGF/FGFR1 bioactivity (17, 18), and soluble α-Klotho overexpression (19, 20). The critical role of FGF23 in phosphate balance is underscored by the fact that excess FGF23 production causes disorders of hypophosphatemia due to heterogeneous genetic defects (21–27). In the converse situation, reduced secretion of bioactive FGF23 results in hyperphosphatemic familial tumoral calcinosis (hfTC) (28–32).

Conflict of interest: KEW receives royalties for licensing the FGF23 gene to Kyowa-Hakko-Kirin Pharmaceutics, Inc.

Submitted: July 25, 2018
Accepted: January 14, 2019
Published: February 21, 2019

Reference information:
JCI Insight. 2019;4(4):e123817.
https://doi.org/10.1172/jci.insight.123817.

In the setting of chronic kidney disease (CKD), serum phosphate levels are largely within normal ranges until end-stage disease (33). With kidney failure, the expression of α-Klotho progressively falls, leading to a situation of FGF23 resistance (34); this in turn, leads to higher circulating FGF23 to attempt to maintain phosphate balance. The physiological price for relatively normal serum phosphate in the setting of CKD is a reduction in 1,25D synthesis, leading to reduced calcium absorption, hypocalcemia, and hyperparathyroidism (35). Although the mechanisms remain unclear, FGF23 is independently associated with a significantly increased odds ratio for CKD patient mortality (36), predicts responses to calcitriol therapy (37), and is linked to development of left ventricular hypertrophy (LVH) (38, 39). Cardiac hypertrophy is a multifactorial and important mechanism of cardiovascular disease (CVD) in CKD that contributes to diastolic dysfunction, congestive heart failure, and sudden death. Compared with a prevalence of less than 20% in the general population, cardiac hypertrophy affects up to 70% of patients during moderate CKD and approaches 90% of patients on dialysis (40). Although elevated FGF23 is associated with cardiac hypertrophy, the extent of soft tissue calcifications (41), anemia (42), tissue hypoxia (43), inflammation (44), and paracrine/autocrine factors such as Wnt-related proteins and other FGFs (45, 46), which likely play significant roles, remains to be determined. Thus, the complete functions of FGF23 in maintaining mineral homeostasis, as well as its potential crosstalk with other metabolic systems in CKD, are not fully understood.

A mouse harboring a conditional *Fgf23* allele (flox-*Fgf23*) was developed to test targeted restriction of FGF23 expression and function in vivo. We previously showed that osteoblast/osteocyte–specific flox-*Fgf23* recombination using *Dmp1*-Cre suppressed circulating bioactive, intact FGF23 (iFGF23) in mice with normal renal function (47). Importantly, this animal was resistant to increasing FGF23 following high-phosphate dietary challenge (47). Additionally, the osteoblast/osteocyte recombined flox-*Fgf23* allele rescued the inappropriately elevated FGF23, as well as the biochemical and skeletal disease in the *Hyp* mouse model of X-linked hypophosphatemia (XLH) (47). Herein, we showed through Cre-mediated targeting that elevated FGF23 is necessary to avoid systemic effects typically associated with hyperphosphatemia during CKD, providing almost complete protection against vascular calcification and subsequent cardiac hypertrophy.

Results

Mineral metabolism during CKD. To determine the role of FGF23 in CKD progression and manifestations, conditional deletion of a flox-*Fgf23* allele was targeted to osteoblasts/osteocytes by breeding to a *Dmp1*-Cre–transgenic line (48) to create flox-*Fgf23*/*Dmp1*-Cre$^{+/-}$ mice. Adenine diet was used to induce CKD (51), and female mice were studied to permit an extended CKD time course for study, as males are known to be far more sensitive to adenine (52). From weaning to 8 weeks of age, the mice were fed a normal rodent chow; mice were then switched to either a control casein-containing diet or a 0.2% adenine–containing diet for 4 or 8 additional weeks. In the 8-week treatment groups, interim bleeds were taken at 4 weeks. To test hormonal responses during CKD, serum intact FGF23 (iFGF23) concentrations were measured. At 4 weeks on the experimental diets, serum bioactive iFGF23 concentrations were significantly elevated in the flox-*Fgf23*/*Dmp1*-Cre^{-} mice fed adenine (Figure 1A). However, the flox-*Fgf23*/*Dmp1*-Cre^{+} mice had significantly lower serum iFGF23 than the flox-*Fgf23*/*Dmp1*-Cre^{-} mice, which remained virtually unchanged at the 8-week time point (Figure 1A). Flox-*Fgf23*/*Dmp1*-Cre^{+} mice receiving adenine had significantly elevated serum iFGF23 over flox-*Fgf23*/*Dmp1*-Cre^{+} and flox-*Fgf23*/*Dmp1*-Cre^{-} mice receiving control diet (Figure 1A). Serum iFGF23 was not different in the control-diet-fed mice (Figure 1A). Consistent with the marked reduction in serum FGF23, cortical bone *Fgf23* mRNA levels were significantly lower (~90%; $P < 0.01$) in the flox-*Fgf23*/*Dmp1*-Cre^{+} mice compared with the flox-*Fgf23*/*Dmp1*-Cre^{-} mice fed adenine at 4 weeks (Figure 1B). At 8 weeks on diet, the flox-*Fgf23*/*Dmp1*-Cre^{+} adenine-fed mice maintained significantly lower *Fgf23* mRNA compared with flox-*Fgf23*/*Dmp1*-Cre^{-} mice (Figure 1B).

Biochemical manifestations of lower FGF23 during CKD. Upon analysis of serum biochemistries, phosphate concentrations were found to be similar between casein-fed flox-*Fgf23*/*Dmp1*-Cre^{-} and /*Dmp1*-Cre^{+} mice at 4 weeks, but a significant difference between the 2 groups at 8 weeks, with flox-*Fgf23*/*Dmp1*-Cre^{+} mice having increased concentrations (Figure 1C). When receiving adenine diet, the flox-*Fgf23*/*Dmp1*-Cre^{+} mice had a significant increase in serum phosphate versus flox-*Fgf23*/*Dmp1*-Cre^{-}littermates at both time points (Figure 1C); serum calcium levels were not different across all genotypes and diets (Table 1). Blood urea nitrogen (BUN) was monitored for decline in renal function, and as expected, adenine diet was associated with a significantly increased BUN, but concentrations were further elevated

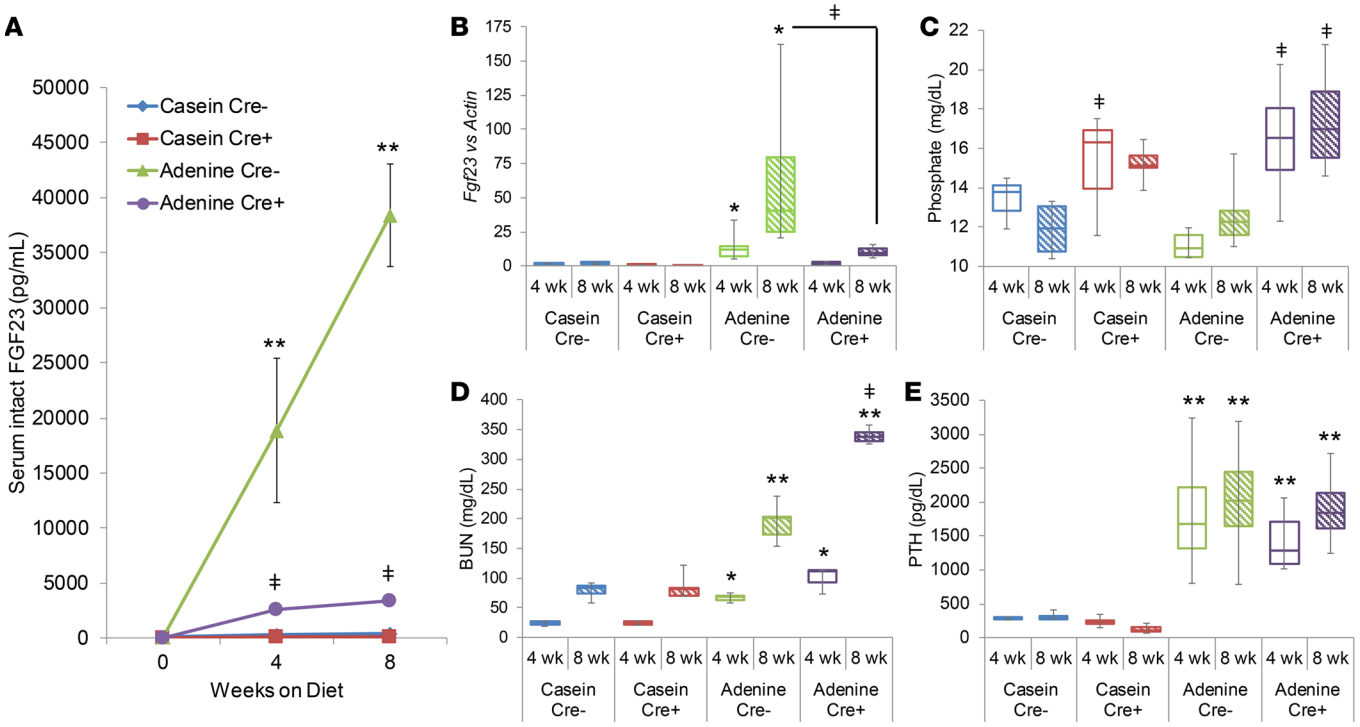

Figure 1. Biochemical and molecular phenotypes of flox-*Fgf23* mice during CKD. (**A**) Flox-*Fgf23*/*Dmp1*-Cre mice were placed on casein control or 0.2% adenine diet for 8 weeks. By 4 weeks on diet, serum intact FGF23 levels were significantly elevated in the mice fed adenine diet, yet the levels in flox-*Fgf23*/*Dmp1*-Cre$^+$ mice were significantly lower than those in the flox-*Fgf23*/*Dmp1*-Cre$^-$ mice, which continued at the 8-week time point. (**B**) Bone *Fgf23* mRNA levels rose in the flox-*Fgf23*/*Dmp1*-Cre$^-$ mice fed adenine at 4 weeks on diet versus casein control. At 8 weeks on diet, the flox-*Fgf23*/*Dmp1*-Cre$^+$ adenine-fed mice had significantly lower *Fgf23* mRNA compared with flox-*Fgf23*/*Dmp1*-Cre$^-$. (**C**) Serum phosphate levels were found to be similar between flox-*Fgf23*/*Dmp1*-Cre$^-$ and flox-*Fgf23*/*Dmp1*-Cre$^+$ mice at 4 weeks on casein, with an increase in the flox-*Fgf23*/*Dmp1*-Cre$^+$ mice at 8 weeks. On adenine diet, the Cre$^+$ mice had a significant increase versus flox-*Fgf23*/*Dmp1*-Cre$^-$ littermates on the adenine diet at both time points. (**D**) Blood urea nitrogen (BUN) levels were measured to monitor renal function. As expected, adenine diet increased these levels, but were further elevated in the Cre$^+$ mice on adenine at the 8-week time point. (**E**) Serum analysis also showed that the adenine diet model induced hyperparathyroidism. All mice receiving adenine had a significant increase in serum PTH compared with the casein control group, even at the 4-week time point. There was no difference between genotypes and there was no further increase at the 8-week time point in the adenine-fed mice (n = 4–6 per group). *P < 0.05, **P < 0.01 versus casein diet within the same genotype; ‡P < 0.05 versus Cre$^-$ on the same diet.

in the flox-*Fgf23*/*Dmp1*-Cre$^+$ mice at the 8-week time point (Figure 1D). Serum creatinine levels paralleled BUN (Table 1). Serum alkaline phosphatase was significantly reduced in the flox-*Fgf23*/*Dmp1*-Cre$^+$ compared with the flox-*Fgf23*/*Dmp1*-Cre$^-$littermates fed either diet (Table 1), but after 8 weeks was significantly elevated in the adenine-fed flox-*Fgf23*/*Dmp1*-Cre$^+$ mice compared with controls. This pattern trended similarly in the flox-*Fgf23*/*Dmp1*-Cre$^-$ mice between diets but did not reach significance (Table 1). Similar to previous reports with adenine administration, serum total iron was significantly reduced in the adenine-fed mice compared with the casein controls after 8 weeks of diet administration. No differences were observed in iron levels between genotypes fed either the casein or adenine diet.

Skeletal and renal phenotypes with CKD and reduced FGF23 expression. Upon analysis of other key hormones involved in the CKD pathogenesis, the adenine diet was noted to induce hyperparathyroidism. Regardless of genotype, all mice receiving adenine had significantly higher serum PTH compared with the casein control group at both the 4- and 8-week time points (Figure 1E). As chronically elevated PTH concentrations are known to increase osteoclast activity, femora underwent micro–computed tomography (μCT) analysis. Mice fed the adenine diet showed increased porosity, and when quantified showed that femoral cortical porosity was significantly higher than casein by even 4 weeks of diet administration (Supplemental Figure 1A; supplemental material available online with this article; https://doi.org/10.1172/jci.insight.123817DS1). Furthermore, there were no differences observed between genotypes (Supplemental Figure 1B). The level of cortical porosity was maintained after 8 weeks of adenine diet administration, with no differences observed between genotypes.

FGF23 is typically a potent suppressor of the renal vitamin D 1α-hydroxylase (*Cyp27b1*) (10), whereas PTH has the converse effect on this enzyme (53). Consistent with elevated PTH, renal expression of

Table 1. Serum biochemical analysis

	4 week				8 week			
	Casein Cre⁻	Casein Cre⁺	Adenine Cre⁻	Adenine Cre⁺	Casein Cre⁻	Casein Cre⁺	Adenine Cre⁻	Adenine Cre⁺
Calcium (mg/dl)	9.58 + 0.28	9.96 + 0.45	8.85 + 0.7	9.15 + 0.4	11.98 + 1.72	11.53 + 0.49	10.85 + 0.32	11.91 + 0.79
Total Iron (μg/dl)	127.16 + 34	133.75 + 31	84.81 + 13	91.03 + 2.5				
Total Iron (μmol/l)					42.38 + 1.5	35.4 + 3.5	20.96 + 1.4[A]	22.50 + 1.4[A]
Alk Phos (U/l)	181 + 14	99.75 + 10[B]	139.4 + 17	108.75 + 13	131.25 + 11	83.40 + 7.8[C]	150.00 + 5.9	125.25 + 6.9[A]
Creatinine (mg/dl)	0.37 + 0.04	0.31 + 0.04	0.55 + 0.08	0.64 + 0.07[B]	0.41 + 0.08	0.45 + 0.03	0.79 + 0.02[A]	0.94 + 0.05[A]

Data presented as mean + SD. n = 4–6 per group. [A]$P < 0.01$ vs. casein diet, same genotype. [B]$P < 0.05$, [C]$P < 0.01$ vs. Cre⁻, same diet.

Cyp27b1 mRNA was increased in all mice fed the adenine diet to a similar extent, despite the highly elevated levels of FGF23 in the flox-*Fgf23/Dmp1*-Cre⁻ adenine-fed groups (Figure 2A). The coreceptor for FGF23, α-Klotho, is found to be reduced during CKD. Indeed, *Klotho* mRNA levels decreased with adenine diet administration by 4 weeks in both genotypes (Figure 2B). After 8 weeks of diet administration, *Klotho* mRNA showed no further decrease in the adenine-fed groups and no differences between genotypes. Over the course of renal damage, fibrotic tissue accumulates, which can be measured by the level of type 1 collagen (Col1a1; Figure 2C). Renal mRNA expression of *Col1a1* is dramatically increased with adenine diet administration by 4 weeks, indicative of renal damage and in line with serum creatinine and BUN levels. However, *Col1a1* levels were not further enhanced with an additional 4 weeks of diet consumption. Additionally, *Col1a1* mRNA levels measured in the adenine-fed flox-*Fgf23/Dmp1*-Cre⁺ group were similar to the adenine-fed flox-*Fgf23/Dmp1*-Cre⁻ mice (Figure 2C). Histological analysis of the kidney demonstrated increased fibrosis and cellular infiltrates within the adenine-fed mice (Figure 2D). Von Kossa staining elucidated mineral deposition, which occurred in all flox-*Fgf23/Dmp1*-Cre⁺ adenine-fed mice and 20% of the flox-*Fgf23/Dmp1*-Cre⁻ adenine-fed animals (Table 2). Expression levels for markers of inflammation including tumor necrosis factor α (*Tnfa*), C-reactive protein (*Crp*), and interleukin-6 (*Il6*) were all found significantly elevated in kidneys from the adenine-fed groups compared with the casein-fed mice (Figure 2, E–G). Interestingly, *Crp* and *Il6* mRNA expression was further enhanced in the flox-*Fgf23/Dmp1*-Cre⁺ adenine-fed mice compared with the adenine-fed flox-*Fgf23/Dmp1*-Cre⁻ mice (Figure 2, F and G). Consistent with mineral accumulation, expression levels of runt-related transcription factor (*Runx2*) were elevated in all animals receiving adenine; however, no differences between genotypes were observed despite higher prevalence of mineral content within the adenine-fed flox-*Fgf23/Dmp1*-Cre⁺ kidneys.

Cardiac morphology with CKD in the context of blunted FGF23 expression. Cardiac hypertrophy in CKD is a multifactorial pathogenesis involving tissue calcification (54), local growth factors (55), as well as a direct role of FGF23 (38). To monitor heart properties during CKD onset, echocardiograph images were collected from the mice prior to the 8-week time point. Representative long-axis images collected in B-mode show the aorta down to the apex of the open left ventricle (Figure 2A). Whereas no gross changes were observed between the genotypes at baseline, the flox-*Fgf23/Dmp1*-Cre⁺ mice fed adenine showed thicker aortic walls with calcification (Figure 3A). Additionally, ejection fraction and fractional shortening were significantly increased in the adenine-fed flox-*Fgf23/Dmp1*-Cre⁺ mice (Table 3). H&E staining of representative hearts from the adenine-fed group showed pronounced hypertrophy of the left ventricle in the flox-*Fgf23/Dmp1*-Cre⁺ mice fed adenine compared with flox-*Fgf23/Dmp1*-Cre⁻ mice (Figure 3B). These mice also contained calcification in the heart tissue; however, they displayed variable locations of accumulation (Supplemental Figure 2). Hypertrophy was also found to occur at the cellular level. Cardiomyocyte cell area increased in mice fed adenine compared with the casein-fed mice and was further increased in the adenine-fed flox-*Fgf23/Dmp1*-Cre⁺ mice (Figure 3C). Thus, high FGF23 over the time-course studies was associated with partial protection from cardiac hypertrophy in this model.

Discussion

In the current work, we found that providing an adenine-containing diet to mice induces renal disease and potently increases FGF23 and PTH, modeling the endocrine profile of patients with CKD. Although targeted deletion of *Fgf23* from osteoblast/osteocytes reduced FGF23 protein and bone mRNA levels 90%, this reduction did not inhibit the incidence of hyperparathyroidism, nor did it prevent the resulting increase in

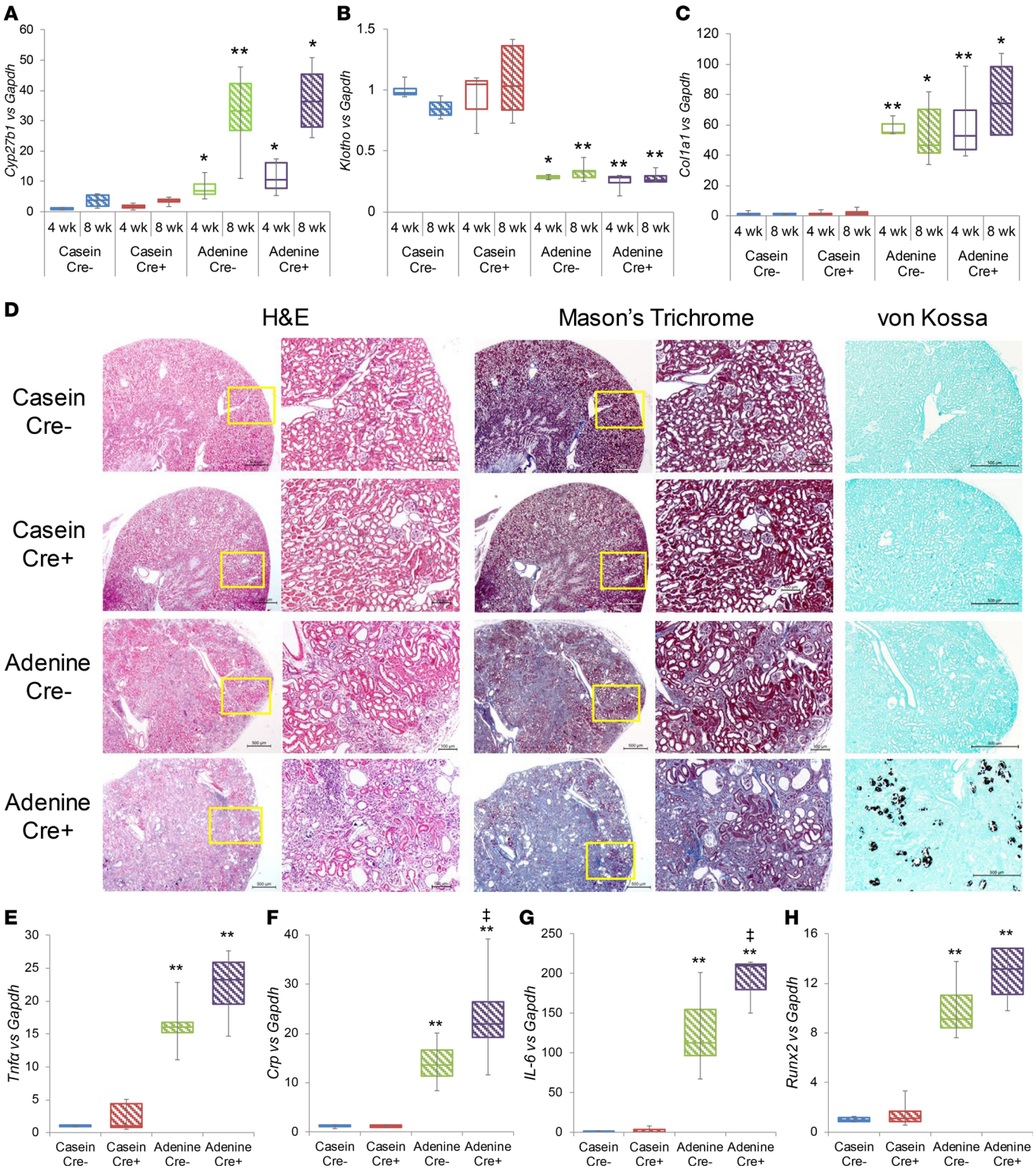

Figure 2. Renal phenotypes under clamped FGF23. (**A**) Consistent with high PTH, renal expression of 1α-hydroxylase (*CYP27b1*) was increased in all mice fed the adenine diet and despite the highly elevated levels of FGF23 in the flox-*Fgf23*/*Dmp1*-Cre$^-$ adenine-fed group. (**B**) Renal *Klotho* mRNA levels were reduced in the adenine-fed mice compared with the casein-fed groups. (**C**) Fibrosis marker *Col1a1* was significantly upregulated with adenine diet administration compared with casein. These levels were maintained by 8 weeks on diet with no differences between genotypes. (**D**) H&E and Masson's trichrome staining of the kidney tissue showed increased cell infiltration and fibrosis within the adenine-fed mice. Mineral accumulation detected by von Kossa staining was most pronounced in the adenine-fed flox-*Fgf23*/*Dmp1*-Cre$^+$ group. Scale bars: 500 μm and 100 μm (insets). (**E**) *Tnfa* mRNA levels were found to be increased in both genotypes fed adenine compared with casein. Expression of inflammation markers *Crp* (**F**) and *Il6* (**G**) mRNA was significantly induced in adenine-fed mice, but was also found at significantly higher levels in the adenine-fed flox-*Fgf23*/*Dmp1*-Cre$^+$ mice compared with the adenine-fed flox-*Fgf23*/*Dmp1*-Cre$^-$ group. (**H**) *Runx2* mRNA expression, related to mineral deposition, was increased in both genotypes fed adenine compared with casein (n = 4–6 per group). *$P < 0.05$, **$P < 0.01$ versus casein diet within the same genotype; ‡$P < 0.05$ versus Cre$^-$ on the same diet.

Table 2. Kidney histological scores

		Number of cases			
I. Fibrosis	**Score**	**Casein Cre⁻**	**Casein Cre⁺**	**Adenine Cre⁻**	**Adenine Cre⁺**
a. None	0	4	4		
b. Patchy	1		1	2	1
c. Severe	2			3	3
II. Glomeruli					
a. Normal	0	4	5	5	3
b. Drop out	1				1
III. Calcification					
a. None	0	4	3	3	
b. Minimal	1			1	
c. Medulla only	2		2		1
d. Cortex and Medulla	3			1	3
IV. Cell infiltrates					
a. None	0	4	4	3	3
b. Present	1		1	2	1

cortical bone porosity. Furthermore, reducing FGF23 during CKD actually resulted in higher serum BUN and phosphorus, as well as more pronounced cardiac hypertrophy. Collectively, these findings demonstrate that during CKD, elevated FGF23 has a critical and potentially protective role, including maintaining systemic phosphate for normal cardiac homeostasis.

FGF23 is a central factor in the pathogenesis of CKD, owing to its impact on endocrine function, as well as its associations with morbidity and mortality in this patient population (36, 56). Under normal physiological circumstances, FGF23 interacts with α-Klotho and FGFR in the kidney to promote phosphate excretion and indirectly decrease intestinal phosphate absorption by reducing 1,25D synthesis. Initial pathogenic insults during CKD lead to relatively rapid suppression of α-Klotho, leading to FGF23 resistance and reduced phosphate clearance (57). Our study herein demonstrated a decrease in renal *Klotho* mRNA expression in adenine-fed mice for 4 weeks, which was similarly suppressed at 8 weeks. Additionally, serum creatinine and BUN rose between 4 and 8 weeks in the adenine-fed mice compared with casein-fed mice, which demonstrates the progressive nature of this model. In a likely compensatory fashion, iFGF23 levels rose, which led to secondary hyperparathyroidism. Interestingly, perhaps due to the competing actions of FGF23 and PTH, the mice fed adenine showed slight elevations in kidney *Cyp27b1*. Even with normal renal function, elevated FGF23 is known to negatively affect bone homeostasis, as underscored by the rachitic phenotype of patients with autosomal dominant hypophosphatemia (ADHR) (21) and X-linked hypophosphatemia (XLH) (58). Recent studies demonstrated that FGF23 neutralization using anti-FGF23 antibodies in the *Hyp* mouse model of XLH (59) or in XLH patients (60) was able to correct serum phosphorus levels to within the normal ranges and improve bone parameters. However, with compromised renal function, use of a neutralizing FGF23 antibody in a rat model of CKD led to the deaths of the animals (61). It was observed that FGF23 neutralization decreased levels of serum PTH and increased circulating levels of 1,25D (62). This resulted in increased uptake of calcium and phosphorus from the diet, leading to markedly increased serum phosphate.

To circumvent the complete blockade of FGF23 activity, in previous work we employed the bone-specific deletion of FGF23 using the conditional flox-*Fgf23* mice (47). Similar to neutralization with anti-FGF23, conditional deletion of *Fgf23* in *Hyp* mice corrected the XLH phenotype. Importantly, when *Fgf23* was deleted using *Dmp1*-Cre for late osteoblasts/early osteocytes, the mice remained modestly responsive to elevated phosphorus (47). Indeed, flox-*Fgf23*/*Dmp1*-Cre$^+$ mice fed an adenine-containing diet in the current study showed increased bone *Fgf23* mRNA and serum iFGF23; however, these levels remained far below those of the adenine-fed flox-*Fgf23*/*Dmp1*-Cre$^-$ mice. In contrast with the aforementioned neutralization studies,

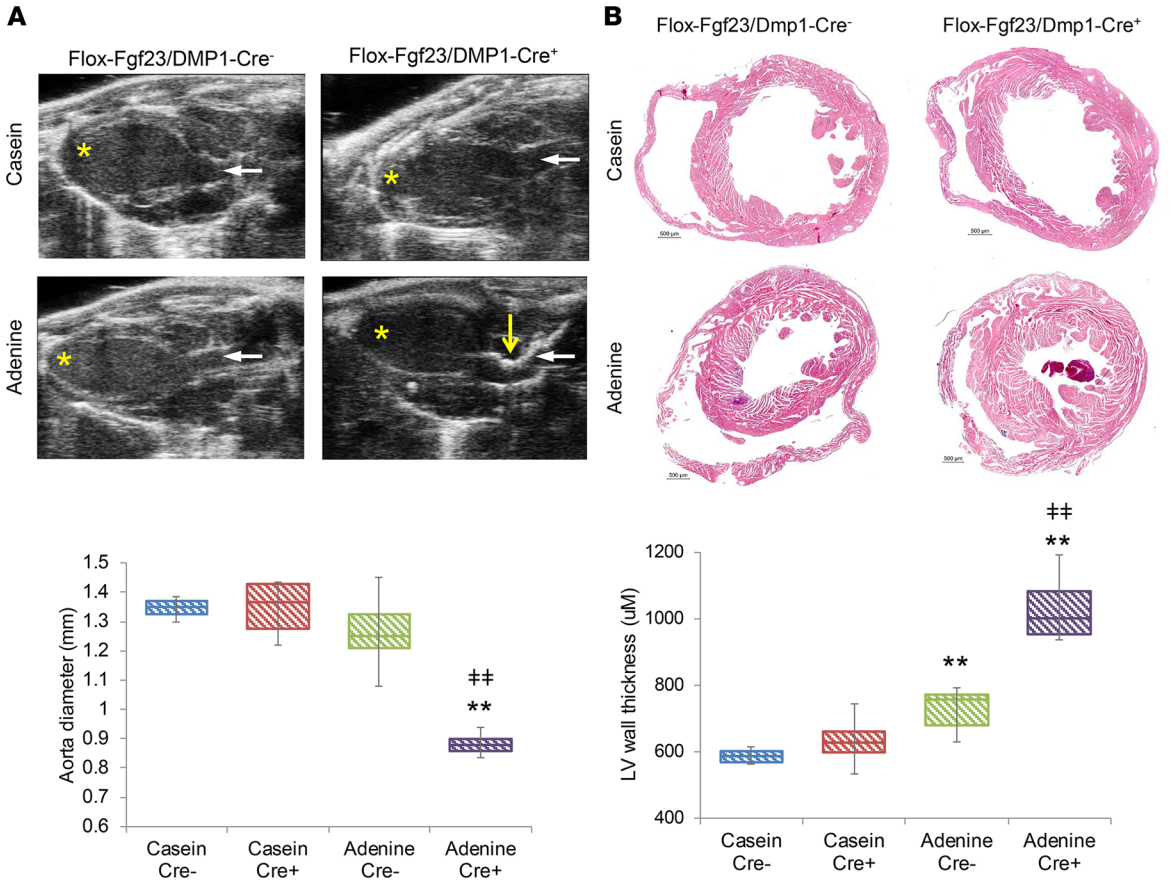

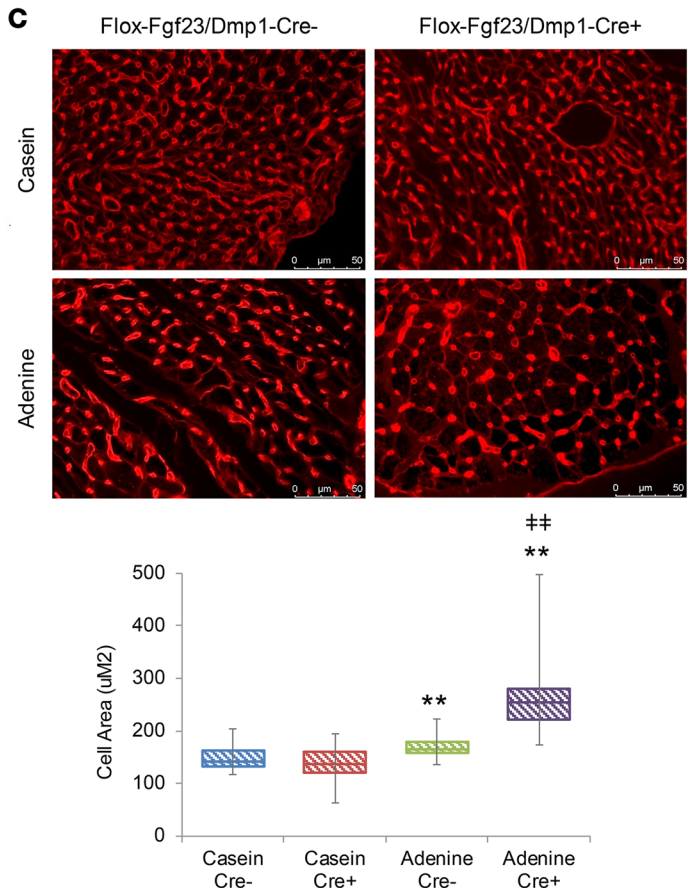

Figure 3. Cardiac phenotypes with clamped FGF23. (**A**) Echocardiograph images were collected from the mice prior to the 8-week time point. Representative long-axis images collected in B-mode show the aorta (right) down to the apex of the open left ventricle (left). While no gross changes were observed between the genotypes at baseline, the flox-*Fgf23/Dmp1*-Cre$^+$ mice fed adenine showed thickened aortic walls due to calcification (yellow arrow). Quantification of the aortic diameter in the lower panel demonstrated significantly lower values in the adenine-fed Cre$^+$ mice. Yellow asterisks indicate the apex of the heart; white arrows indicate the aorta to denote similar orientation for each image. (**B**) Representative H&E staining of casein- and adenine-fed hearts demonstrates pronounced hypertrophy of the left ventricle in the flox-*Fgf23/Dmp1*-Cre$^+$ mice fed adenine compared with the flox-*Fgf23/Dmp1*-Cre$^-$ mice. Lower panel: Whereas no differences were observed between genotypes on the casein diet, left ventricle wall thickness was higher in the adenine-fed flox-*Fgf23/Dmp1*-Cre$^+$ mice compared with both casein-fed mice and adenine-fed flox-*Fgf23/Dmp1*-Cre$^-$ mice (n = 4–6 per group). $^{**}P < 0.01$ versus casein diet within the same genotype; $^{‡‡}P < 0.01$ versus flox-*Fgf23/Dmp1*-Cre$^-$ on the same diet. (**C**) Wheat germ agglutinin staining of the cardiomyocytes demonstrated an increase in cell area, a marker of hypertrophy, in the adenine-fed flox-*Fgf23/Dmp1*-Cre$^-$ mice (lower panel). In the flox-*Fgf23/Dmp1*-Cre$^+$ adenine-fed group, cell area was significantly increased compared with both casein controls as well as the adenine-fed flox-*Fgf23/Dmp1*-Cre$^-$ mice (n = 30–40 images per group). $^{**}P < 0.01$ versus casein diet within the same genotype; $^{‡‡}P < 0.01$ versus Cre$^-$ on the same diet.

Table 3. Echocardiography parameters

	Casein Cre⁻	Casein Cre⁺	Adenine Cre⁻	Adenine Cre⁺
LVID/s	2.87 + 0.08	2.89 + 0.11	2.89 +1.8	1.74 + 0.38[A,B]
LVPW/s	0.83 + 0.03	0.86 + 0.04	0.89 + 0.04	1.25 + 0.11[A,B]
EF%	48.8 + 2.2	50.9 + 2.9	47.2 + 4.7	73.6 + 12[C]
FS%	24.2 + 1.3	25.6 + 1.7	23.6 + 2.9	45.6 + 10.5[C,D]

LVID/s, left ventricle inner diameter in systole; LVPW/s, left ventricle posterior wall in systole; EF, ejection fraction; FS, fractional shortening. Data presented as mean + SD. n = 4–6/group. [A]$P < 0.01$ vs. casein diet, same genotype. [B]$P < 0.01$, [C]$P < 0.05$ vs. Cre⁻, same diet. [D]$P < 0.05$ vs. casein diet, same genotype.

serum PTH levels were similar between the adenine-fed Cre⁻ and Cre⁺ groups. It is possible that even the dramatic decrease of iFGF23 was unable to elicit changes in circulating 1,25D resulting in the secondary rise of PTH. The increase in mortality of the CKD rats with anti-FGF23 treatment was partially attributed to declines in renal function. In agreement with this finding, our study found that after 8 weeks of diet administration the flox-*Fgf23/Dmp1*-Cre⁺ mice receiving adenine had substantially higher serum BUN compared with both casein-fed flox-*Fgf23/Dmp1*-Cre⁺ mice and the adenine-fed flox-*Fgf23/Dmp1*-Cre⁻ mice.

FGF23 has been independently associated with increased risk for all-cause mortality in CKD patients (36) through increased incidence of cardiovascular events (63), the leading cause of death in this patient population (64). Animal models with direct heart injections or intravenous infusion of high-dose recombinant FGF23, as well as *Klotho*-null mice with elevated serum iFGF23, develop LVH, an index of heart dysfunction and a frequent abnormality found in end-stage renal disease patients (38, 65–67). Additionally, various animal models of CKD develop LVH, including adenine diet administration (68), 5/6 nephrectomy (66), and *Col4a3*$^{-/-}$ mice (model of Alport syndrome; ref. 69); however, these are not always consistent, also relying upon the genetic background of the mice. In our hands, the hypertrophy of the adenine diet in the flox-*Fgf23/Dmp1*-Cre⁻ mice was modest over the 8-week time course. Interestingly, the adenine-fed flox-*Fgf23/Dmp1*-Cre⁺ mice showed significant LVH at 8 weeks of diet administration by histology. This supports the concept that development of LVH in CKD is multifactorial and not solely dependent on markedly elevated serum iFGF23. Indeed, even with global ablation of FGF23, LVH can be induced through pressure overload (70). Serum phosphorus was increased in all of the adenine-fed mice; however, the levels were highest in the flox-*Fgf23/Dmp1*-Cre⁺ mice. In our studies, echocardiographs also showed a decrease in aortic width in the adenine-fed flox-*Fgf23/Dmp1*-Cre⁺ mice from mineral accumulation. In the previous report of CKD rats treated with anti-FGF23 neutralizing antibody, the authors observed increased vascular calcifications compared with the vehicle-treated CKD rats, which was also attributed to the elevated serum phosphorus. In contrast to our results, however, heart weight and LVH were unchanged between the vehicle- and anti-FGF23–treated CKD rats (61). These differences could potentially be explained by the differences in duration of hyperphosphatemia and extent of vascular calcifications, rodent-specific local factors, or the endocrine profiles of the 2 models. Exposure to high serum phosphorus has been shown to cause dedifferentiation of the vascular smooth muscle cells into osteoblast-like cells that inappropriately deposit matrix material (71). The arterial stiffness caused by this mineralized material increases the demands on the heart, resulting in hypertrophy (72). Additionally, in vitro experiments have demonstrated that treatment of cardiomyocytes with exogenous phosphate can directly induce hypertrophic signals (73). Reduced 1,25D and vitamin D receptor signaling within cardiomyocytes has also been shown to induce hypertrophy (74, 75). Although the cardiac hypertrophy in the adenine-fed flox-*Fgf23/Dmp1*-Cre⁻ mice was modest, it is possible that the change in 1,25D from iFGF23 reduction was not sufficient to block cardiomyocyte hypertrophy in the adenine-fed flox-*Fgf23/Dmp1*-Cre⁺ mice. Additionally, high serum PTH has been associated with cardiovascular events and it was shown that treatment with PTH for 2 weeks after transverse aortic banding decreased heart function and increased heart size (76). Thus, it is possible that the high serum PTH in the adenine-fed flox-*Fgf23/Dmp1*-Cre⁺ mice could contribute to the development of LVH. Finally, Slavic et al. have shown that after transverse aortic constriction, heart tissue and cardiomyocytes can express FGF23 (70). This may act in an autocrine or paracrine manner within the heart by signaling through FGFR4 and inducing hypertrophy through the PLC-γ/NFAT/calcineurin pathway (66). It is therefore possible that there is a compensatory upregulation

of FGF23 within cardiomyocytes in the adenine-fed flox-*Fgf23*/*Dmp1*-Cre^{+} mice. Future studies will be needed to assess cardiomyocyte signaling events during CKD utilizing heart conditional deletion of *Fgf23*.

Bone homeostasis in CKD is also severely affected; a combination of increased cortical porosity and reduced bone quality in CKD patients increases fracture risk, independently increasing morbidity and mortality (77–80). In this study, we found that the adenine-fed mice, along with the alterations in mineral homeostasis, incurred elevated cortical porosity compared with the casein-fed mice. Unlike the FGF23 neutralization studies, the bones from mice fed the adenine diet showed no improvement with osteoblast/osteocyte deletion of FGF23. Chronic PTH in CKD elicits high bone turnover that was alleviated with anti-FGF23 treatment, likely due to reduced PTH (61). The improved bone in the rat CKD studies was likely due to the observation that neutralization of FGF23 reduced serum PTH, whereas PTH was not different between the adenine-fed flox-*Fgf23*/*Dmp1*-Cre^{-} and flox-*Fgf23*/*Dmp1*-Cre^{+} groups herein. We hypothesize that this is the reason that cortical porosity was not improved despite FGF23 reduction.

In summary, we found that FGF23 is protective during CKD by acting to maintain serum phosphate in the normal ranges. Inhibition of FGF23 during kidney disease onset results in elevated serum phosphorus, more severe renal disease, and cardiac hypertrophy. It is likely that other factors in addition to serum phosphate increase FGF23 during CKD; thus, it will be necessary to determine the balance of circulating FGF23 concentrations that permit adequate phosphate handling but potentially limit detrimental, off-target events.

Methods

Animal studies. Flox-*Fgf23* mice were derived as described previously (47).

Conditional deletion of the flox-Fgf23 allele. Heterozygous flox-*Fgf23* (*Fgf23*$^{fl/+}$) mice were bred to generate *Fgf23*$^{fl/fl}$/Cre$^{+/-}$ mice using the 8-kb dentin matrix protein 1 (*Dmp1*)-Cre (48) transgenic mouse line. All genotype analyses were performed as previously described (47).

Rodent diets. Mice were weaned at 3 weeks of age. Beginning at 8 weeks of age, mice were provided a control casein-base rodent diet (0.9% phosphate and 0.6% calcium, TD.150303 Envigo). To induce CKD, littermates were placed on a 0.2% adenine–containing diet supplemented into the casein base (TD.160020; Envigo), until sacrifice after 4 and 8 weeks on diets; group sizes were 4–7 animals. Diets and water were provided ad libitum.

Cardiac analysis. Three days prior to harvest, experimental mice underwent echocardiography imaging. Mice were anesthetized with isoflurane and placed on a warming mat with continuous monitoring. Transthoracic ECHO images were obtained using a VisualSonics 2100 ultrasound machine for small-animal imaging and MS400 transducer (Fujifilm VisualSonics, Inc.). A 40-MHz hand-held mechanical transducer containing both imaging (B-mode) and Doppler transducers with a frame rate of 34 Hz was used to image the heart in multiple views and measure aortic diameter. M-mode–captured transaxial images of the left ventricle were used to determine left ventricle width measurements and calculate ejection fraction and fractional shortening. At necropsy, hearts were fixed in 4% paraformaldehyde (PFA). Heart volume and myocardial calcification were evaluated using iodine potassium iodide (I2KI) tissue staining and μCT imaging. Hearts were placed in 1 ml of Lugol's solution, aqueous potassium iodide plus iodine (Sigma Aldrich, L6146) for 24 hours, and then returned to 1 ml of neutral buffered formalin. I2KI-stained hearts were dabbed dry to remove residual solution, and then scanned (Skyscan, 1172) at a resolution of 9 μm while wrapped in Parafilm to reduce sample dehydration. A threshold was applied to the volume of interest to define myocardium (VOI 20–75) and myocardial calcification (VOI 75–255). Graphic renderings of hearts were generated (CTVox, Bruker) with myocardium defined as red and myocardium calcification as white. All hearts were subsequently paraffin embedded and transverse sections at 7-μm thickness were stained with H&E. Images were stitched on a Leica microscope at ×5 magnification. ImageJ (NIH) was used to determine left ventricular wall thickness by taking 7 measurements of the left ventricle free wall from each sample. Sections were deparaffinized and stained with Alexa Fluor 488–conjugated wheat germ agglutinin (Life Technologies). Fluorescence images were captured on a Leica microscope at ×20 magnification with 8–10 left ventricle free wall images per sample. ImageJ was used to measure the cell area from 50–100 cells per image.

Kidney histology. At necropsy, kidneys were perfused with 0.9% saline and 4% PFA for fixation. Paraffin-embedded 7-μM sections were stained with H&E, Masson's trichrome for fibrosis, and von Kossa with methyl green counterstain for imaging mineral deposition. Histology scores were semiquantitatively assessed in 3 sections per specimen in a blinded manner by an experienced nephrologist. Images were captured on a Leica microscope at ×2.5 and ×10 magnifications. Analyses were done by comparing those without and with any calcification.

Serum biochemistries. Blood samples were collected from mice for interim analyses by facial vein bleed and at the time of euthanasia by cardiac puncture. Routine serum biochemistries were determined in the Laboratory of the Clinical and Translational Sciences Institute (CTSI) of the Indiana University School of Medicine using an automated COBAS MIRA Plus Chemistry Analyzer (Roche Diagnostics). Serum total iron measures ferric iron bound to transferrin, which was processed and analyzed according to the manufacturer's protocol (Randox Laboratories). Serum iFGF23 and intact PTH concentrations were assessed using commercial ELISAs (Quidel, Inc.).

μCT. Femurs were removed after necropsy and fixed in 4% PFA. Bones were scanned using μCT (Skyscan 1172) at 6-μm micron resolution to assess trabecular and cortical bone morphometry. A defined region of interest in the distal femur (~0.5 mm from the growth plate and encompassing 1 mm of slices in the proximal direction) was used to determine trabecular bone volume/total volume (BV/TV). A single cortical bone slice (2 mm proximal to the most proximal slice defined for trabecular analysis) was analyzed for cortical porosity by isolating the cortical shell and determining void space (100 – [BV/TV]). The terminology and units used are those recommended by the American Society for Bone and Mineral Research Guidelines for assessment of bone microstructure in rodents using μCT (49).

RNA preparation and quantitative RT-PCR (qPCR). Kidneys and bones were harvested and homogenized in 1 ml of TRIzol reagent (Invitrogen) according to the manufacturer's protocol using a Bullet Blender (Next Advance, Inc.), then further purified using the RNeasy Kit (Qiagen). RNA samples were tested with intron-spanning primers specific for *Fgf23* (bone), *Cyp27b1*, *Col1a1*, *Tnfa*, *Crp*, *Il6*, *Runx2*, and *Klotho* (kidney) mRNAs; mouse *β-actin* or *Gapdh* was used as an internal control by RT-qPCR. The qPCR primers and probes were purchased as pre-optimized reagents (Applied Biosystems/Life Technologies, Inc.) and the TaqMan One-Step RT-PCR kit was used to perform qPCR. PCR conditions for all experiments were 30 minutes 48°C, 10 minutes 95°C, followed by 40 cycles of 15 seconds 95°C and 1 minute 60°C. The data were collected and analyzed by a StepOne Plus system (Applied Biosystems/Life Technologies, Inc.). The expression levels of mRNAs were calculated relative to appropriate littermate genotype controls, and the $2^{-\Delta\Delta CT}$ method described by Livak was used to analyze the data (50).

Statistics. Statistical analysis of the in vivo and in vitro data was performed by 2-way ANOVA followed by Tukey's post hoc test. Statistical significance for all tests was set at $P < 0.05$. Data are presented as box-and-whisker plots, where the middle line represents the median of the data, upper and lower quartiles are within the boxes, and the whiskers are the minimum and maximum.

Study approval. Animal studies were approved by and performed according to the Institutional Animal Care and Use Committee (IACUC) of Indiana University, and comply with the NIH guidelines for the use of animals in research.

Author contributions

ELC and KEW contributed to the study design. ELC, MLN, PN, JCT, JMH, MA, EAS, SMM, and MRA collected and analyzed data. ELC, SMM, MRA, and KEW wrote, and critically revised the final draft of the manuscript.

Acknowledgments

The authors would like to acknowledge NIH grants R21-AR059278, R01-DK112958, R01-DK063934, R01-DK95784 (to KEW), and F32-AR065389 (to ELC); the Indiana Genomics Initiative (INGEN), supported in part by the Lilly Endowment, Inc.; The David Weaver Professorship and a Showalter Scholar award through the Ralph W. and Grace M. Showalter Research Trust (to KEW). The authors also thank Anthony Acton for assistance with biochemical analyses.

Address correspondence to: Erica L. Clinkenbeard or Kenneth E. White, Department of Medical and Molecular Genetics, Indiana University School of Medicine, 975 West Walnut St., IB130, Indianapolis, Indiana 46202, USA. Phone: 317.278.1775; Email: eclinken@iu.edu (ELC); kenewhit@iupui.edu (KEW).

1. Tenenhouse HS, Econs MJ. Mendelian hypophosphatemias. In: Valle D, ed. *The Metabolic and Molecular Bases of Inherited Disease*. New York, NY: The McGraw-Hill Companies; 2001:5039–5068.
2. White KE, Larsson TE, Econs MJ. The roles of specific genes implicated as circulating factors involved in normal and disordered phosphate homeostasis: frizzled related protein-4, matrix extracellular phosphoglycoprotein, and fibroblast growth factor

23. *Endocr Rev*. 2006;27(3):221–241.
3. Burnett SM, Gunawardene SC, Bringhurst FR, Jüppner H, Lee H, Finkelstein JS. Regulation of C-terminal and intact FGF-23 by dietary phosphate in men and women. *J Bone Miner Res*. 2006;21(8):1187–1196.
4. Antoniucci DM, Yamashita T, Portale AA. Dietary phosphorus regulates serum fibroblast growth factor-23 concentrations in healthy men. *J Clin Endocrinol Metab*. 2006;91(8):3144–3149.
5. Perwad F, Azam N, Zhang MY, Yamashita T, Tenenhouse HS, Portale AA. Dietary and serum phosphorus regulate fibroblast growth factor 23 expression and 1,25-dihydroxyvitamin D metabolism in mice. *Endocrinology*. 2005;146(12):5358–5364.
6. Shimada T, et al. FGF-23 is a potent regulator of vitamin D metabolism and phosphate homeostasis. *J Bone Miner Res*. 2004;19(3):429–435.
7. Kurosu H, et al. Regulation of fibroblast growth factor-23 signaling by klotho. *J Biol Chem*. 2006;281(10):6120–6123.
8. Urakawa I, et al. Klotho converts canonical FGF receptor into a specific receptor for FGF23. *Nature*. 2006;444(7120):770–774.
9. Shimada T, et al. Cloning and characterization of FGF23 as a causative factor of tumor-induced osteomalacia. *Proc Natl Acad Sci USA*. 2001;98(11):6500–6505.
10. Larsson T, et al. Transgenic mice expressing fibroblast growth factor 23 under the control of the alpha1(I) collagen promoter exhibit growth retardation, osteomalacia, and disturbed phosphate homeostasis. *Endocrinology*. 2004;145(7):3087–3094.
11. Lyles KW, Drezner MK. Parathyroid hormone effects on serum 1,25-dihydroxyvitamin D levels in patients with X-linked hypophosphatemic rickets: evidence for abnormal 25-hydroxyvitamin D-1-hydroxylase activity. *J Clin Endocrinol Metab*. 1982;54(3):638–644.
12. Liu S, et al. Fibroblast growth factor 23 is a counter-regulatory phosphaturic hormone for vitamin D. *J Am Soc Nephrol*. 2006;17(5):1305–1315.
13. Rhee Y, et al. Parathyroid hormone receptor signaling in osteocytes increases the expression of fibroblast growth factor-23 in vitro and in vivo. *Bone*. 2011;49(4):636–643.
14. Farrow EG, et al. Iron deficiency drives an autosomal dominant hypophosphatemic rickets (ADHR) phenotype in fibroblast growth factor-23 (Fgf23) knock-in mice. *Proc Natl Acad Sci USA*. 2011;108(46):E1146–E1155.
15. Rickard DJ, et al. Intermittent treatment with parathyroid hormone (PTH) as well as a non-peptide small molecule agonist of the PTH1 receptor inhibits adipocyte differentiation in human bone marrow stromal cells. *Bone*. 2006;39(6):1361–1372.
16. Weiss RA. Virulence and pathogenesis. *Trends Microbiol*. 2002;10(7):314–317.
17. Hryszko T, Rydzewska-Rosolowska A, Brzosko S, Koc-Zorawska E, Mysliwiec M. Low molecular weight iron dextran increases fibroblast growth factor-23 concentration, together with parathyroid hormone decrease in hemodialyzed patients. *Ther Apher Dial*. 2012;16(2):146–151.
18. Chen NX, O'Neill KD, Allen MR, Newman CL, Moe SM. Low bone turnover in chronic kidney disease is associated with decreased VEGF-A expression and osteoblast differentiation. *Am J Nephrol*. 2015;41(6):464–473.
19. Smith RC, et al. Circulating αKlotho influences phosphate handling by controlling FGF23 production. *J Clin Invest*. 2012;122(12):4710–4715.
20. Hum JM, et al. Chronic hyperphosphatemia and vascular calcification are reduced by stable delivery of soluble klotho. *J Am Soc Nephrol*. 2017;28(4):1162–1174.
21. ADHR Consortium. Autosomal dominant hypophosphataemic rickets is associated with mutations in FGF23. *Nat Genet*. 2000;26(3):345–348.
22. White KE, Carn G, Lorenz-Depiereux B, Benet-Pages A, Strom TM, Econs MJ. Autosomal-dominant hypophosphatemic rickets (ADHR) mutations stabilize FGF-23. *Kidney Int*. 2001;60(6):2079–2086.
23. [No authors listed]. A gene (PEX) with homologies to endopeptidases is mutated in patients with X-linked hypophosphatemic rickets. The HYP Consortium. *Nat Genet*. 1995;11(2):130–136.
24. Jonsson KB, et al. Fibroblast growth factor 23 in oncogenic osteomalacia and X-linked hypophosphatemia. *N Engl J Med*. 2003;348(17):1656–1663.
25. Liu S, Zhou J, Tang W, Jiang X, Rowe DW, Quarles LD. Pathogenic role of Fgf23 in Hyp mice. *Am J Physiol Endocrinol Metab*. 2006;291(1):E38–E49.
26. Tagliabracci VS, et al. Dynamic regulation of FGF23 by Fam20C phosphorylation, GalNAc-T3 glycosylation, and furin proteolysis. *Proc Natl Acad Sci USA*. 2014;111(15):5520–5525.
27. Liu P, et al. Specific ablation of mouse Fam20C in cells expressing type I collagen leads to skeletal defects and hypophosphatemia. *Sci Rep*. 2017;7(1):3590.
28. Topaz O, et al. Mutations in GALNT3, encoding a protein involved in O-linked glycosylation, cause familial tumoral calcinosis. *Nat Genet*. 2004;36(6):579–581.
29. Larsson T, et al. Fibroblast growth factor-23 mutants causing familial tumoral calcinosis are differentially processed. *Endocrinology*. 2005;146(9):3883–3891.
30. Larsson T, et al. A novel recessive mutation in fibroblast growth factor-23 causes familial tumoral calcinosis. *J Clin Endocrinol Metab*. 2005;90(4):2424–2427.
31. Ichikawa S, et al. A homozygous missense mutation in human KLOTHO causes severe tumoral calcinosis. *J Clin Invest*. 2007;117(9):2684–2691.
32. Bergwitz C, et al. Defective O-glycosylation due to a novel homozygous S129P mutation is associated with lack of fibroblast growth factor 23 secretion and tumoral calcinosis. *J Clin Endocrinol Metab*. 2009;94(11):4267–4274.
33. Levin A, et al. Prevalence of abnormal serum vitamin D, PTH, calcium, and phosphorus in patients with chronic kidney disease: results of the study to evaluate early kidney disease. *Kidney Int*. 2007;71(1):31–38.
34. Hu MC, et al. Klotho deficiency causes vascular calcification in chronic kidney disease. *J Am Soc Nephrol*. 2011;22(1):124–136.
35. Miyauchi M, et al. Visible-light-sensitive photocatalysts: nanocluster-grafted titanium dioxide for indoor environmental remediation. *J Phys Chem Lett*. 2016;7(1):75–84.
36. Gutiérrez OM, et al. Fibroblast growth factor 23 and mortality among patients undergoing hemodialysis. *N Engl J Med*. 2008;359(6):584–592.
37. Kazama JJ, et al. Pretreatment serum FGF-23 levels predict the efficacy of calcitriol therapy in dialysis patients. *Kidney Int*.

2005;67(3):1120–1125.
38. Faul C, et al. FGF23 induces left ventricular hypertrophy. *J Clin Invest*. 2011;121(11):4393–4408.
39. Prost S, Sheahan S, Rannie D, Harrison DJ. Adenovirus-mediated Cre deletion of floxed sequences in primary mouse cells is an efficient alternative for studies of gene deletion. *Nucleic Acids Res*. 2001;29(16):E80.
40. Di Lullo L, Gorini A, Russo D, Santoboni A, Ronco C. Left ventricular hypertrophy in chronic kidney disease patients: from pathophysiology to treatment. *Cardiorenal Med*. 2015;5(4):254–266.
41. Moe SM. Calcium as a cardiovascular toxin in CKD-MBD. *Bone*. 2017;100:94–99.
42. Akaishi M, et al. Effect of anemia correction on left ventricular hypertrophy in patients with modestly high hemoglobin level and chronic kidney disease . *J Cardiol*. 2013;62(4):249–256.
43. Zoccali C, et al. Left ventricular hypertrophy and nocturnal hypoxemia in hemodialysis patients. *J Hypertens*. 2001;19(2):287–293.
44. Gupta J, et al. Association between inflammation and cardiac geometry in chronic kidney disease: Findings from the CRIC study. *PLoS ONE*. 2015;10(4):e0124772.
45. Fan J, et al. Recombinant frizzled1 protein attenuated cardiac hypertrophy after myocardial infarction via the canonical Wnt signaling pathway. *Oncotarget*. 2018;9(3):3069–3080.
46. Santiago JJ, et al. High molecular weight fibroblast growth factor-2 in the human heart is a potential target for prevention of cardiac remodeling. *PLoS ONE*. 2014;9(5):e97281.
47. Clinkenbeard EL, et al. Conditional deletion of murine Fgf23: Interruption of the normal skeletal responses to phosphate challenge and rescue of genetic hypophosphatemia. *J Bone Miner Res*. 2016;31(6):1247–1257.
48. Yang W, et al. Dentin matrix protein 1 gene cis-regulation: use in osteocytes to characterize local responses to mechanical loading in vitro and in vivo. *J Biol Chem*. 2005;280(21):20680–20690.
49. Roskoski R. Janus kinase (JAK) inhibitors in the treatment of inflammatory and neoplastic diseases. *Pharmacol Res*. 2016;111:784–803.
50. Livak KJ, Schmittgen TD. Analysis of relative gene expression data using real-time quantitative PCR and the 2(-delta delta C(T)) Method. *Methods*. 2001;25(4):402–408.
51. Jia T, et al. A novel model of adenine-induced tubulointerstitial nephropathy in mice. *BMC Nephrol*. 2013;14:116.
52. Diwan V, Small D, Kauter K, Gobe GC, Brown L. Gender differences in adenine-induced chronic kidney disease and cardiovascular complications in rats. *Am J Physiol Renal Physiol*. 2014;307(11):F1169–F1178.
53. Bajwa A, Forster MN, Maiti A, Woolbright BL, Beckman MJ. Specific regulation of CYP27B1 and VDR in proximal versus distal renal cells. *Arch Biochem Biophys*. 2008;477(1):33–42.
54. Kitamura K, et al. Relationship between cardiac calcification and left ventricular hypertrophy in patients with chronic kidney disease at hemodialysis initiation. *Heart Vessels*. 2017;32(9):1109–1116.
55. Corda S, et al. Trophic effect of human pericardial fluid on adult cardiac myocytes. Differential role of fibroblast growth factor-2 and factors related to ventricular hypertrophy. *Circ Res*. 1997;81(5):679–687.
56. Isakova T, et al. Fibroblast growth factor 23 and risks of mortality and end-stage renal disease in patients with chronic kidney disease. *JAMA*. 2011;305(23):2432–2439.
57. Koh N, et al. Severely reduced production of klotho in human chronic renal failure kidney. *Biochem Biophys Res Commun*. 2001;280(4):1015–1020.
58. Hruska KA, Rifas L, Cheng SL, Gupta A, Halstead L, Avioli L. X-linked hypophosphatemic rickets and the murine Hyp homologue. *Am J Physiol*. 1995;268(3 Pt 2):F357–F362.
59. Tokarz D, Martins JS, Petit ET, Lin CP, Demay MB, Liu ES. Hormonal regulation of osteocyte perilacunar and canalicular remodeling in the Hyp mouse model of X-linked hypophosphatemia. *J Bone Miner Res*. 2018;33(3):499–509.
60. Carpenter TO, et al. Randomized trial of the anti-FGF23 antibody KRN23 in X-linked hypophosphatemia. *J Clin Invest*. 2014;124(4):1587–1597.
61. Shalhoub V, et al. FGF23 neutralization improves chronic kidney disease-associated hyperparathyroidism yet increases mortality. *J Clin Invest*. 2012;122(7):2543–2553.
62. Sun N, et al. FGF23 neutralization improves bone quality and osseointegration of titanium implants in chronic kidney disease mice. *Sci Rep*. 2015;5:8304.
63. Nakano C, et al. Intact fibroblast growth factor 23 levels predict incident cardiovascular event before but not after the start of dialysis. *Bone*. 2012;50(6):1266–1274.
64. Eckardt KU, et al. Evolving importance of kidney disease: from subspecialty to global health burden. *Lancet*. 2013;382(9887):158–169.
65. Mirza MA, Larsson A, Melhus H, Lind L, Larsson TE. Serum intact FGF23 associate with left ventricular mass, hypertrophy and geometry in an elderly population. *Atherosclerosis*. 2009;207(2):546–551.
66. Grabner A, et al. Activation of cardiac fibroblast growth factor receptor 4 causes left ventricular hypertrophy. *Cell Metab*. 2015;22(6):1020–1032.
67. Leifheit-Nestler M, et al. Induction of cardiac FGF23/FGFR4 expression is associated with left ventricular hypertrophy in patients with chronic kidney disease. *Nephrol Dial Transplant*. 2016;31(7):1088–1099.
68. Shobeiri N, Pang J, Adams MA, Holden RM. Cardiovascular disease in an adenine-induced model of chronic kidney disease: the temporal link between vascular calcification and haemodynamic consequences. *J Hypertens*. 2013;31(1):160–168.
69. Neuburg S, et al. Genetic background influences cardiac phenotype in murine chronic kidney disease. *Nephrol Dial Transplant*. 2018;33(7):1129–1137.
70. Slavic S, et al. Genetic ablation of Fgf23 or Klotho does not modulate experimental heart hypertrophy induced by pressure overload. *Sci Rep*. 2017;7(1):11298.
71. Giachelli CM. Vascular calcification: in vitro evidence for the role of inorganic phosphate. *J Am Soc Nephrol*. 2003;14(9 Suppl 4):S300–S304.
72. Toussaint ND, Kerr PG. Vascular calcification and arterial stiffness in chronic kidney disease: implications and management. *Nephrology (Carlton)*. 2007;12(5):500–509.
73. Hu MC, et al. Klotho and phosphate are modulators of pathologic uremic cardiac remodeling. *J Am Soc Nephrol*.

2015;26(6):1290–1302.
74. Achinger SG, Ayus JC. The role of vitamin D in left ventricular hypertrophy and cardiac function. *Kidney Int Suppl*. 2005;(95):S37–42.
75. Xiang W, et al. Cardiac hypertrophy in vitamin D receptor knockout mice: role of the systemic and cardiac renin-angiotensin systems. *Am J Physiol Endocrinol Metab*. 2005;288(1):E125–E132.
76. Cha H, et al. Parathyroid hormone accelerates decompensation following left ventricular hypertrophy. *Exp Mol Med*. 2010;42(1):61–68.
77. Alem AM, et al. Increased risk of hip fracture among patients with end-stage renal disease. *Kidney Int*. 2000;58(1):396–399.
78. Mittalhenkle A, Gillen DL, Stehman-Breen CO. Increased risk of mortality associated with hip fracture in the dialysis population. *Am J Kidney Dis*. 2004;44(4):672–679.
79. Jamal SA. Bone mass measurements in men and women with chronic kidney disease. *Curr Opin Nephrol Hypertens*. 2010;19(4):343–348.
80. Babayev R, Nickolas TL. Bone disorders in chronic kidney disease: an update in diagnosis and management. *Semin Dial*. 2015;28(6):645–653.